J. Chin. Inst. Chem. Engrs., Vol. 36, No. 4, 311-320, 2005

Morphological Transitions of Shallow Cells during Thin-Film Solidification of an Alloy: Phase Field Modeling & Experimental Observation

Chi-Jen Shih[1], Wei-Tze Hsu[2], and Chung-Wen Lan[3]

Department of Chemical Engineering, National Taiwan University
Taipei 106, Taiwan

Abstract—The morphological transitions of shallow cells near the onset of Mullins-Sekerka instability during the thin-film directional solidification of a succinonitrile/acetone alloy have been simulated quantitatively by means of phase field modeling for the first time. Long time/length scale experiments at a constant pulling speed were performed for the purpose of comparison. The simulation results show good agreement with classic theories in the planar and $\lambda_c \leftrightarrow \lambda_c/2$ cellular bifurcation regions, where λ_c is the critical wavelength. At a higher pulling speed, V, an anti-trapping current was introduced to maintain the local equilibrium, and the region for $V\lambda^2$~constant was found. Finally, multiplets appeared when λ was close to $\lambda_c/4$. In the experiments, due to slow solute accumulation in the molten zone, morphological transitions were also revealed. Some interesting nonlinear phenomena, such as tip splitting, coarsening, pinch-off, and asymmetric cells, were also confirmed through both simulations and experiments.

Key Words : Phase field simulation, Morphological instability, Directional solidification

INTRODUCTION

The morphological transition that occurs during thin-film alloy solidification near the onset of instability is one of the most important research topics related to pattern formation in materials science and physics. The planar interface becomes unstable at a certain critical value of the control parameter, which is either the pulling speed (V) or the temperature gradient (G), as described by the classical Mullins-Sekerka (MS) theory (Mullins and Sekerka, 1964). This morphological instability occurs because the constitutional supercooling overcomes the stabilizing effects of the thermal gradient and interfacial tension. As observed in experiments, once instability starts, shallow cellular structures begin to grow followed by the growth of deep cells and then dendrites as the speed increases and thermal gradients decrease. Among the above transitions, shallow cells have very rich nonlinear dynamics. However, despite many theoretical (Mullins and Sekerka, 1964; Warren and Langer, 1993), experimental (Eshelman and Trivedi, 1987; Eshelman *et al.*, 1988; Kurowski and Trivedi, 1989) and computational (Ungar and Brown, 1984; Tsiveriotis and Brown, 1993; Lee *et al.*, 1992) studies in this topic, the long-time scale morphological transitions of shallow cells are still not clearly understood. In addition, the mutual dependence between the wavelength and the pulling speed after the critical point is not clear.

For a given thermal gradient, the critical wavelength (λ_c) and pulling speed (V_c) can be predicted by the MS theory (Mullins and Sekerka, 1964). However, because of the narrow range of the control parameters for shallow cells, in addition to a long molten zone (on the order of D_l/V, where D_l is the solute diffusivity) and high purity sample, precise control of the pulling speed is required for shallow-cell observation (Lee *et al.*, 1992). As shown by the theoretical analysis of Warren and Langer (WL) (1993), the interface position takes a very long time (on order of D_l/kV^2, where k is the segregation coefficient) to reach a steady state. Near the onset of instability, the solidification speed is small, so the time scale for morphological dynamics becomes extremely large. Therefore, detailed experiments on shallow cellular transitions with a time scale of up to several D_l/kV^2 have not yet been reported. Lee *et al.* (1992) made the first attempt to use a large-scale thin-film solidification system, but shallow cellular wavelengths and morphological evolution as a function of the pulling speed and time were not addressed experimentally.

The front-tracking modeling with bifurcation analysis performed by Brown's group (Ungar and Brown, 1984; Tsiveriotis and Brown, 1993; Lee *et*

[1] 施智仁
[2] 徐爲哲
[3] 藍崇文, To whom all correspondence should be addressed

al., 1992) provided the first insights into the morphological transition of shallow cells. They showed that the shallow cellular transition is a mode selection that occurs through the bifurcation of $\lambda_c \rightarrow \lambda_c/2 \rightarrow \lambda_c/4$ (Lee *et al.*, 1992). The accompanying local time-periodic amplitude oscillation has also been illustrated (Tsiveriotis and Brown, 1993). However, Eshelman *et al.* (1988) showed experimentally that $V\lambda^2$ is approximately a constant, which differs from the findings of Brown's group; the amplitude variation at the primary bifurcation is subcritical (Eshelman and Trivedi, 1987). In addition, because the front-tracking technique requires grid deformation and local mapping, it is much more difficult to simulate problems that involve interface merging or separation, such as tip splitting, coarsening, and pinching off (Kurowski *et al.*, 1989). Hence, large-scale simulation of global morphological dynamics is still very challenging.

The phase field model has emerged as a powerful tool for simulating solidification problems with complex morphological evolution (Lan *et al.*, 2002, 2004; Ahmad *et al.*, 1998; Boettinger and Warren, 1999; Bi and Sekerka, 2002; Provatas *et al.*, 1999). However, quantitative simulation of alloy solidification is not trivial. An extremely small interface thickness (in order of 0.1 μm) is required for thermodynamic consistency, while a large domain (>1000 μm) is needed to accommodate the solute boundary layer and characteristic wavelength. Because of the restriction on the interface thickness, the time scales in the previous phase field modeling studies (Ahmad *et al.*, 1998; Boettinger and Warren, 1999; Bi and Sekerka, 2002) on directional solidification were small, on the order of a few microseconds, even when an adaptive mesh refinement (AMR) scheme was employed (Provatas *et al.*, 1999; Lan *et al.*, 2002). These factors make comparisons between simulations and experiments extremely difficult. In addition, at higher speeds, solute trapping (Ahmad *et al.*, 1998; Aziz and Kaplan, 1988) can be induced due to the diffusive interface of the phase field, and the value of the "effective segregation coefficient" k_{eff} deviates from the equilibrium value (k) dramatically with increasing speed (Ahmad *et al.*, 1998). Fortunately, Karma (2001) has proposed an "anti-trapping current" (ATC) to suppress this kinetic effect. Recently, Lan and Shih (2004) applied it to the WBM model (Warren and Boettinger, 1995) and simulated quantitatively binary alloy dendritic growth in a forced flow.

In this study, we present some interesting results for shallow cellular transitions and dynamics studied through quantitative phase field modeling and long-time scale thin-film solidification experiments on a succinonitrile (SCN)/acetone alloy. To reduce the computational load, the solute concentration used in the simulations was set at 0.01 mol%, which is much lower than that employed in the experiments (0.151 mol%). As a result, the time for dynamic evolution was significantly reduced. In addition, phase field parameters and thermodynamic properties were selected to maintain the local equilibrium (k=0.1, m= –222 K/mol frac.), and the concept of ATC was adopted to achieve higher pulling speeds. To observe long-time scale phenomena up to several D_L/kV^2 in the experiments, growth cell was designed to be sufficiently large, and the pulling speed was controlled precisely with a micro-stepping motor. With a constant pulling speed, the solute accumulated slowly along the interface, and so as the bulk melt concentration (c_0), due to the finite molten zone length. Consequently, detailed morphological planar-to-cellular transitions could be produced without changing the pulling speed. Although the acetone concentration was quite different between the simulations and experiments, the results showed that the overall morphological transitions were very alike. Both quantitative phase field simulations and long-time scale experiments were carried out at a constant pulling speed for the first time. In the next section, the adaptive phase field model and the experimental system will be described briefly. Then result and a discussion are presented which will be followed by conclusions.

ADAPTIVE PHASE FIELD SIMULATION AND EXPERIMENTAL SYSTEM

The phase field simulations performed here were based on the WBM model (Warren and Boettinger, 1995), while the anti-trapping current (ATC) proposed by Karma (2001) was also considered in calculations involving high growth speeds. In our previous study (Lan and Shih, 2004), we used this model to perform quantitative simulations of dendritic growth, and the effects of the interface thickness were investigated. This ATC term introduced for the WBM model in Lan and Shih (2004) was not derived as rigorously as was the one in Karma (2001). However, with tuning of the ATC coefficient, the calculated results with a thicker interface were consistent with the results obtained with a much thinner interface. Consistent local supercoolings and grow speeds with classical solutions could also be obtained. Nevertheless, this model still has a weak point. Because the solutal boundary layer was very thin due to the high tip velocity of the dendrite in our precious report (Lan and Shih, 2004), the solutal profile in front of the dendrite tip was found not to be realistic. This could be a concern when using this ATC term. Fortunately, for shallow cellular growth, due to the much lower growth speed and, thus, much

thicker solutal boundary layer (as compared with the interface thickness) with this ATC correction, a correct solute profile can still be obtained; in addition, the ATC correction is also of course small. Although the use of this ATC should not be a great concern, we prefer to stick with the traditional WBM model as much as possible if the solute trapping is not large. In this study, the ATC correction was used only when the pulling speed was higher than 200 μm/s. Even without ATC compensation, in the worse case encountered here, the effective segregation coefficient (~0.14) was still not very different from the equilibrium value (0.1). At high speeds, the ATC term considered here, though not the best choice, was found to be useful for improving the simulations. The calculated results were consistent with those obtained using a smaller interface thickness.

To present the governing equations in dimensionless form, the variables are rescaled here, and the equations are recast in a moving frame with a constant pulling speed, V. The concentration (atomic fraction), c, is rescaled by the far field concentration, c_0, to obtain c^*. The coordinates x and y are rescaled by the interface thickness, δ, to obtain x^* and y^*, respectively, and time t is scaled by δ^2/D_L to t^*. The phase filed variable ϕ is set to be 1 in the liquid, 0 in the solid, and 0.5 at the interface. The steady solidification speed V is rescaled by D_l/δ to V^*. Then, the governing equations can be represented in dimensionless form as

$$\frac{\partial \phi}{\partial t^*} - V^* \frac{\partial \phi}{\partial y^*} = M_\phi^* \varepsilon^{*2} \left[\nabla \cdot \left(\eta^2 \nabla \phi \right) - \frac{\partial}{\partial x^*} \left(\eta \eta_\beta \frac{\partial \phi}{\partial y^*} \right) + \frac{\partial}{\partial y^*} \left(\eta \eta_\beta \frac{\partial \phi}{\partial x^*} \right) \right] - M_\phi^* S^*, \tag{1}$$

$$\frac{\partial c^*}{\partial t^*} - V^* \frac{\partial c^*}{\partial y^*} = \nabla \cdot \left\{ D^* [\nabla c + c^* (1 - c_0 c^*)(S_B^* - S_A^*) \nabla \phi] + j_a^* \right\}. \tag{2}$$

The physical properties of pure SCN and acetone can be applied to form an ideal alloy solution assumed in the WBM model. The only exception is the latent heat of acetone. It is modified (9.651×10^7 J/m^3) to fit the measured segregation coefficient k (0.1) and the liquidus slope m (–222 K/(mol fraction)). In addition, M_ϕ^*, ε^*, D^*, and S^* are the dimensionless mobility, the parameter related to the interfacial energy, the diffusivity, and the entropy of the alloy, accounting for the mixing rule for the melt and solid. Also, S_A^* and S_B^* are the normalized entropies of A (solvent) and B (solute), respectively. The definitions of these phase field parameters can be found elsewhere (Lan and Shih, 2004; Warren and Boettinger, 1995). The anisotropic function, η, in Eq. (1) is defined for four-fold symmetry as

$$\eta = 1 + \gamma \cos 4\beta, \tag{3}$$

where γ is the intensity of the anisotropy (0.04 is used) and $\beta = \tan^{-1}[(\partial\phi/\partial y)/(\partial\phi/\partial x)]$ is the angle between the local interface position and the pulling orientation. The interface thickness, δ, is chosen to be 0.2 μm to minimize solute trapping and balance the computational load.

The only difference between our approach and the original WBM model (Warren and Boettinger, 1995) is the anti-trapping current j_a^* in the concentration equation, which was proposed by Karma (2001). In the moving frame, j_a^* can be defined as

$$j_a^* = a(1-k) \left[\frac{2c^*}{1 + k - (1-k)h(\phi)} \right] \left(\frac{\partial \phi}{\partial t^*} - V^* \frac{\partial \phi}{\partial y^*} \right) \frac{\nabla \phi}{|\nabla \phi|}. \tag{4}$$

In the present simulations, the ATC coefficient $a = 1/\sqrt{2}$ to make sure that k_{eff} is always smaller than 0.14. A detailed discussion of this ATC term in the WBM model can be found elsewhere (Lan and Shih, 2004).

The simulations were performed for SCN with 0.01 mol% acetone at a thermal gradient of 100 K/cm. A computational domain of 200 μm(W) × 300 μm(H) was considered (see Fig. 1(a)), while the frozen temperature approximation (FTA) with a constant thermal gradient, G, was adopted by neglecting the latent heat as a working assumption. The system can be regarded as a domain having continuous feeding from the top, flowing out from the bottom, as sketched on Fig. 1 (a). On both sides of the domain, the symmetry (no flux) condition is used ($\partial\phi/\partial x^* = 0$, $\partial c^*/\partial x^* = 0$). At the top boundary, the concentration is specified (c^*=1), while at the lower boundary the exit condition is used, *i.e.*, $\partial c^*/\partial y^* = 0$. To solve these equations, an adaptive finite volume method (Lan *et al.*, 2002) was used. During calculation, the mesh was adaptively refined and coarsened along the interface and high concentration-gradient regions, while the minimum grid size Δx was kept at 0.78δ. The maximum number of finite volumes was about 50,000, depending on the complexity of the morphology, and all the calculations were performed on a personal computer (Pentium-4 2G CPU with 512 Mbytes of DDR RAM).

For the experiments, a thin-film directional solidification system was designed for the purpose of long-time scale morphological observation. This system is similar to the one reported by Lee *et al.* (1992) and is depicted in Fig. 1(b). The growth cell was formed between two Pyrex glass plates (6.6×100×

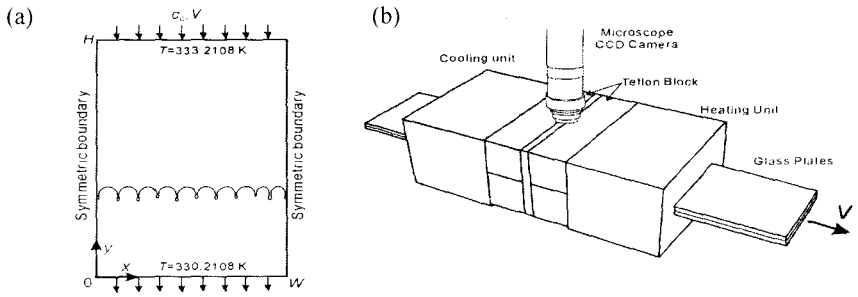

Fig. 1. (a) Schematic of the computational domain for phase field modeling of directional solidification in a moving frame, V; (b) schematic of the long-time scale thin-film directional solidification system.

520 mm^3). The gap of the cell was controlled by a 70 μm-thickness Teflon gasket at the edges. A copper heating unit and a cooling unit were then used, and the detailed temperature distribution near the interface was measured with a K-type thermocouple. The hair-thin thermocouple was placed between the glass plates, translating from the hot to cold zones for temperature recording. An SCN/acetone solution was injected into the cell. To prepare the solution, an ultra-pure SCN sample was purified by means of vacuum distillation for ten times and with 4-pass zone refining for more than 60 runs before the acetone was injected; the zone-refining speed was kept at 1cm/h. Furthermore, before the growth was observed, the sample was repeatedly melted and quenched (more than ten times) until the growth direction [100] was parallel to that of heat flow (y direction). Then, the system was stopped and settled for two days for solute mixing before observations were made. Because of the long growth cell, the growth time of up to several D_L/kV^2 could be reached. In this study, an SCN sample with 0.151 mol% acetone and a thermal gradient of 23.5 K/cm were used. The pulling speed was kept at 1 μm/s, the growth time was more than 36 h (~10 D_L/kV^2), and the total translation distance was about 13 cm. In addition, the concentration (0.151 mol%) was doubly checked based on the MS theory (Mullins and Sekerka, 1964).

RESULTS AND DISCUSSION

Planar interface

According to the MS theory (Mullins and Sekerka, 1964), under a known thermal gradient, the planar interface becomes unstable and wrinkled at a wavelength λ when the pulling speed is larger than some critical value. In the present simulations (c_0=0.01 mol% and G=100 K/cm), the lowest critical speed, V_c, was 72.6 μm/s, which corresponds to a critical wavelength, λ_c, of 68.4 μm. Therefore, before the morphological study was conducted, the planar interface needed to be examined first to check

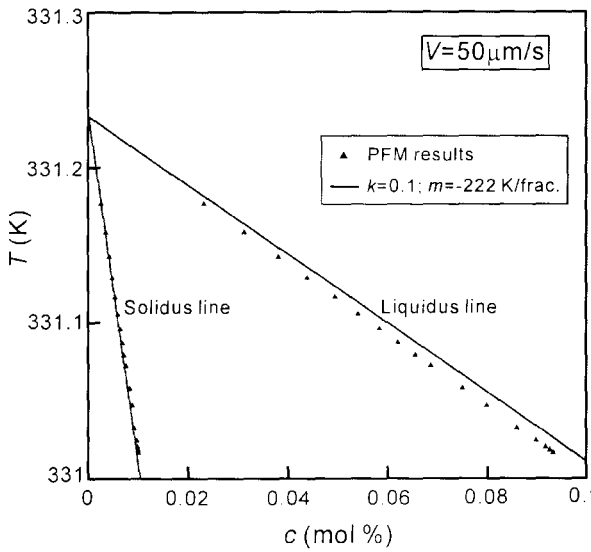

Fig. 2. Comparison of the calculated solid and liquid concentrations based on phase field simulation results for planar solidification at V=50 μm/s with the dilute SCN/Acetone phase diagram (k=0.1; m= −222 K/mol frac.).

the thermodynamic consistency and phase field parameters. At a pulling speed of 50 μm/s, a planar interface was indeed obtained under the given initial conditions (liquid concentration c_L^*=1, solid concentration c_S^*=0.1, and interface temperature T_I= 331.2108 K). Because of the low speed compared with the interface diffusion rate (on the order of D_L/δ, ~0.5 cm/s), ATC was found to not be necessary. As solidification proceeded, the interface moved back and solute was rejected from the interface, but the interface remained planar. During the simulation, both solid and liquid concentrations were also recorded to check the phase equilibrium. As shown in Fig. 2, the kinetic effect induced by the diffuse interface was small and the effective segregation coefficient, k_{eff} ($=c_S/c_L$=0.106), was very close to the equilibrium value (0.1). In addition, the steady-state liquid concentration profile in front of the interface, which is an exponential-decay function, agreed very well with the exact one.

The calculated diffusion distance and interface

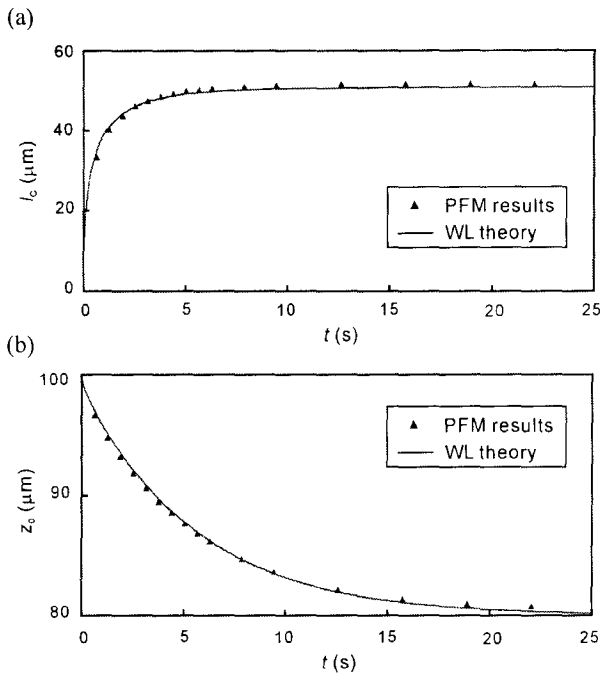

Fig. 3. (a) Calculated characteristic diffusion length l_c; (b) interface position z_0 obtained through phase field simulation (symbols) and from the WL theory (solid line); V=50 μm/s.

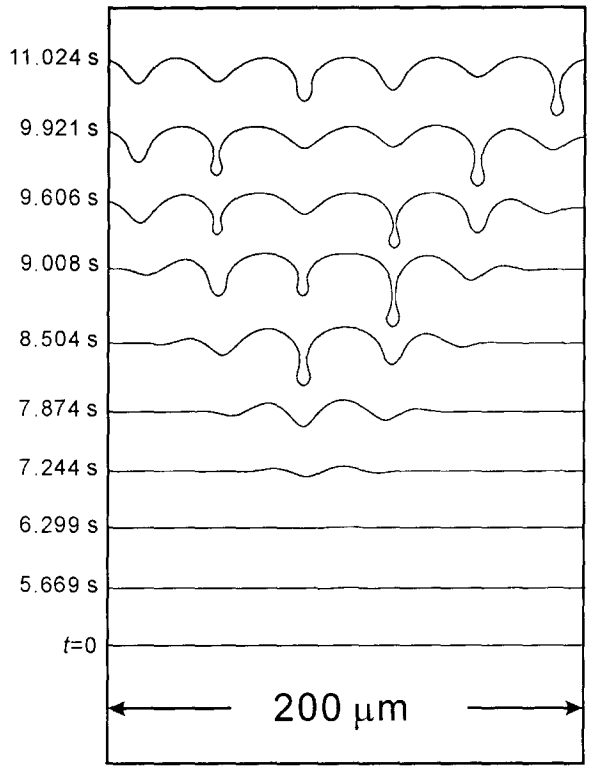

Fig. 4. Phase field simulation of the morphological development of shallow cells from planar to $\lambda_c/2$ structures at a speed of V=100 μm/s.

position were further compared with the analytical solution proposed by Warren and Langer (WL) (1993). They derived a set of coupled ordinary differential equations for the dynamic interface position and solute boundary layer thickness to improve the MS theory. Losert *et al.* (1998) also verified their results experimentally. In our simulations, the results also showed excellent agreement with the WL theory as illustrated in Figs. 3(a) and 3(b), where l_c is the characteristic diffusion length and z_0 is the interface position. From Fig. 3(b), it is clear that the interface position needed to be at least 2 D_L/kV^2 (10.2 s) to approach a steady state. In other words, for an experiment with a pulling speed of V~1 μm/s, a steady interface morphology requires several hours to develop. To avoid the solute accumulation effect in the bulk melt, a much lower solute concentration and large molten zone are necessary. Based on this quantitative comparison, we were confident that we could get reliable results at higher pulling speeds, as long as k_{eff} was close enough to k.

$\lambda_c \leftrightarrow \lambda_c/2$ cellular transitions

As the pulling speed was increased to 90 μm/s, the interface remained planar even up to 10 D_L/kV^2 (15.68 s). However, when the speed was further increased to 100 μm/s, as shown in Fig. 4, the interface became unstable after $5D_L/kV^2$ (6.3 s). A bump appeared and then propagated like a wave along the interface. A fully developed morphology required an additional $5D_L/kV^2$, and the steady wavelength was about 33.3 μm, which is a typical $\lambda_c/2$ mode (λ_c=68.4 μm). The overall development of the shallow cells shown in Fig. 4 is quite similar to that observed in previous experiments (Trivedi and Somboonsuk, 1985).

The speed was further increased stepwise up to 160 μm/s and then backwards to 75 μm/s to check the evolution of the morphological wavelength and amplitude (the distance from the top to the groove of a cell). For all of the speeds considered here, again the time needed to reach a steady state was about 5 D_L/kV^2. The average amplitude (A) has been measured and summarized elsewhere (Lan *et al.*, 2004). The λ_c mode could only be obtained by reducing the pulling speed, and there was a sudden increase in the cell depth when the speed was changed from 85 (a $\lambda_c/2$ mode) to 80 μm/s (a λ_c mode). The planar interface was obtained again when the speed was reduced to 75 μm/s, which gave a rather good prediction of V_c, as compared with the one predicted by the linear stability theory (72.6 μm/s). Furthermore, it is interesting that the amplitude variation is time-periodic, as pointed out by Tsiveriotis and Brown (1993). This local nonlinear behavior at V=140 μm/s has also been described elsewhere (Lan *et al.*, 2004; Lan, 2004). As observed by Kurowski *et al.* (1989) experimentally, the bottom package of the solute was pinched off when the maximum amplitude was reached, and the pinch-off frequency depended on

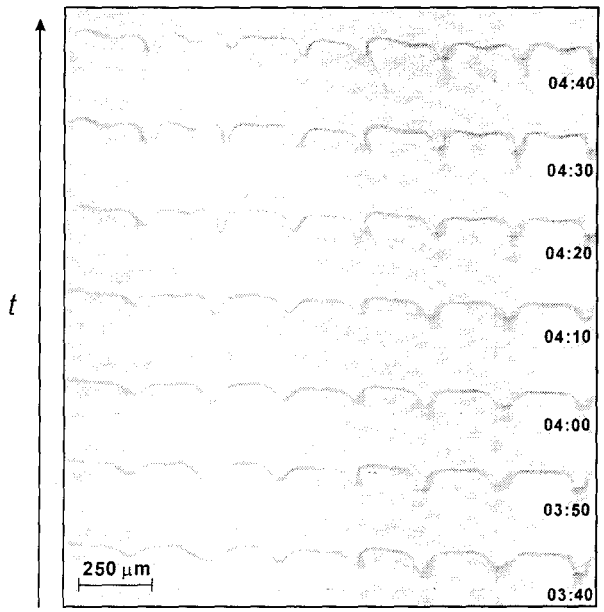

Fig. 5. Experimental observation of $\lambda_c/2$ sallow cells.

the pulling speed. Again, solute trapping was found not to be obvious until the speed reached 160 μm/s. The maximum effective segregation coefficient here was still less than 0.12, so the ATC term was not included in this region.

Interestingly, shallow cells with a $\lambda_c/2$ (λ_c=510 μm) were also observed in our experiments after four hours (about D_l/kV^2) from a planar interface, as shown in Fig. 5. However, because of the extremely narrow region of such shallow cells, this mode was sustained for only about 1 h before turning into cells having a smaller wavelength through tip splitting. The change of the far-field concentration during this one-hour evolution time was believed to be small (<0.5%). Indeed, as predicted by the MS loop, the window needed to get the $\lambda_c/2$ mode was very small (Lan *et al.*, 2004). Therefore, even with a very long molten zone, choosing a precise pulling speed to get the $\lambda_c/2$ mode is not easy. Using a constant pulling speed with a long molten zone seems to be a good approach for observing the detailed morphological change from a planar interface to a $\lambda_c/2$ shallow cellular mode. The λ_c mode can be observed by reducing the pulling speed to a value close to V_c. However, we have not been able to find this mode so far by using the present setup.

Region for $V\lambda^2$ ~ constant

The bifurcation analysis performed by Tsiveriotis and Brown (1993) indicated that the $\lambda_c/4$ branch appears right after the $\lambda_c/2$ mode, which is similar to the transition of $\lambda_c \rightarrow \lambda_c/2$. However, some wavelengths between $\lambda_c/2$ and $\lambda_c/4$ were observed experimentally (Eshelman *et al.*, 1988), where $V\lambda^2$ was approximately a constant. To observe the morphological transition in detail, simulations at higher speeds and experiments with longer times were further conducted here.

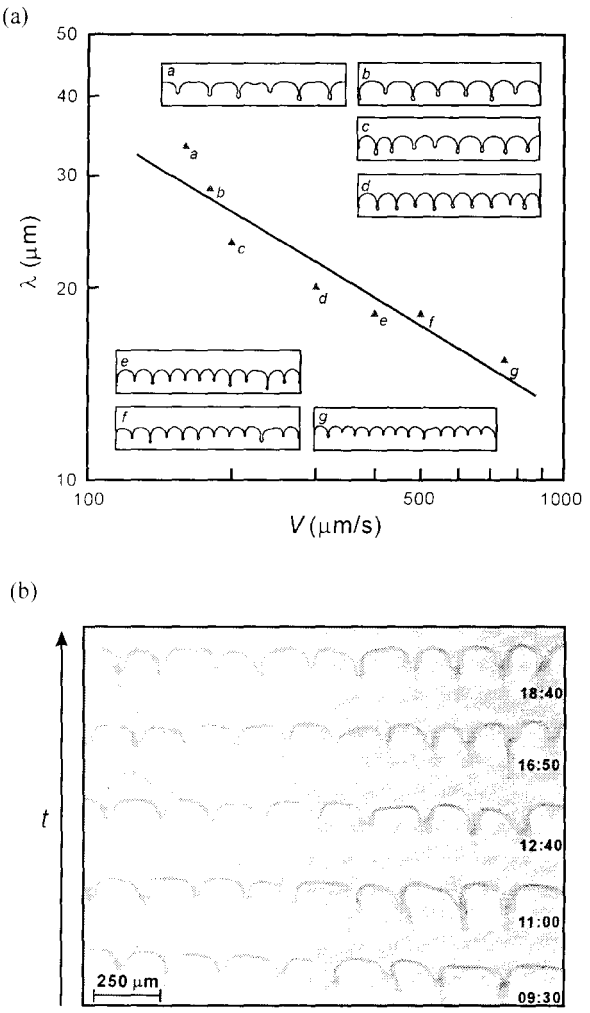

Fig. 6. (a) Variation of simulated wavelengths with pulling speeds between $\lambda_c/2$ and $\lambda_c/4$; $V\lambda^2$ is approximately a constant; (b) experimental observation of some shallow cells having wavelengths between $\lambda_c/2$ and $\lambda_c/4$.

Cells with shorter wavelengths were obtained in simulations as the speed was increased from 160 to 180 μm/s, and it was found that clear global tip splitting, coarsening, and pinching off occurred during the transition. The long-time nonlinear morphological transition and amplitude variation have been discussed in detail elsewhere (Lan *et al.*, 2004). However, when we further increased the speed stepwise to 750 μm/s, we observed a rapid increase of k_{eff} due to solute trapping. Hence, the ATC term was introduced to suppress this trapping phenomena. As mentioned previously, this current keeps the simulated partition from increasing with the velocity, thus making the calculation more quantitative. Even without ATC, the simulated results were acceptable. The amount of ATC correction used here improved the simulation. Wavelengths at different pulling

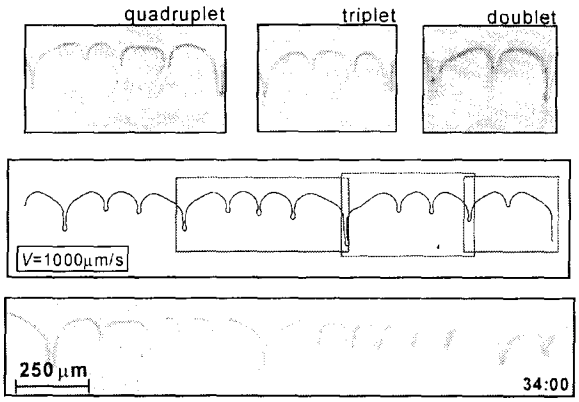

Fig. 7. Comparison of simulated multiplets at V=1000 μm/s with observed ones.

speeds were calculated and are plotted in Fig. 6(a), where some steady-state morphologies were also illustrated. Interestingly, the linear correlation gives $V\lambda^2$~constant, where some wavelength deviations may be caused by the finite domain width used here and discussed by Bi and Sekerka (2002).

In our experiments, shallow cells having shorter wavelengths between $\lambda_c/2$ (255 μm) and $\lambda_c/4$ (128 μm) were also obtained. As shown in Fig. 6(b), five sample morphologies with average wavelengths of 206, 194, 184, 171, and 160 μm were captured, and the sustained time of these wavelengths was much longer (about 15 h) than that in the $\lambda_c/2$ mode. Therefore, this mode should be observed more easily, even in experiments with a much shorter length/time scale (Eshelman *et al.*, 1988; Eshelman, and Trivedi, 1987; Kurowski *et al.*, 1989; Trivedi and Somboonsuk, 1985). In short, the results of both phase field simulations and experiments indicate that the shallow cellular transition after the $\lambda_c/2$ mode is not a mode bifurcation, and that $V\lambda^2$~constant seems to be a good description of the transition.

Multiplets

Jamgotchian *et al.* (1993) first discovered an array of doublets, which are believed to represent a branch of cellular solutions. They pointed out that the speed range of doublets is very narrow, and doublets usually appear when shallow cells are transforming into deep cells. Kopczynski *et al.* (1997) further proposed other multiplets solutions, such as triplets and quadruplets, numerically; a front tracking method using the boundary integral was employed. In their analysis, the multiplets are unique branches that may not coexist, and they are transitional states from shallow to long cellular morphologies.

We also observed these multiplets at V= 1000 μm/s in our simulations and at t= 24 h in our experiments. However, these branches appeared together, as shown in Fig. 7, in which doublet, triplet, and

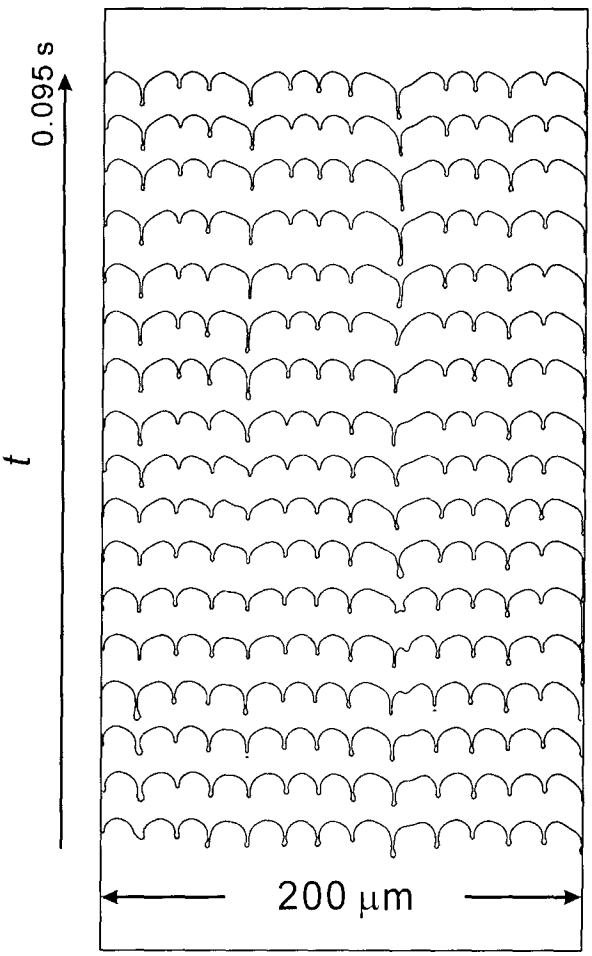

Fig. 8. Morphological transition following a step change of the pulling speed from 750 to 1000 μm/s.

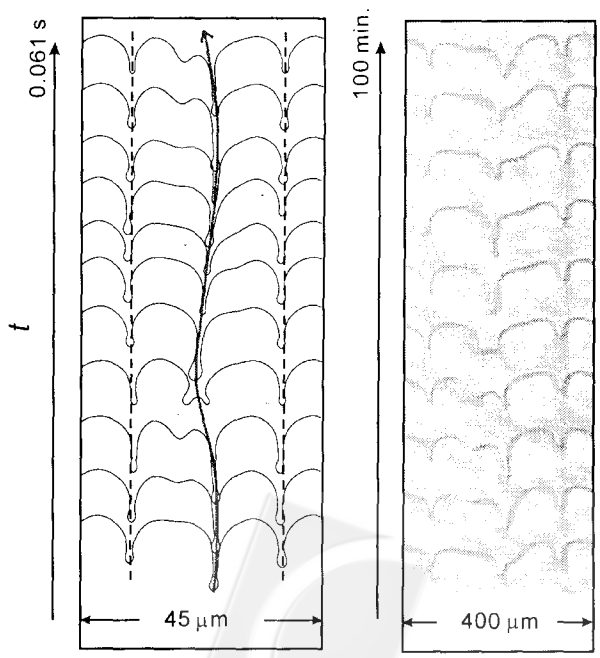

Fig. 9. Simulated (left) (V=750 μm/s) and observed (right) evolution of asymmetric shallow cells.

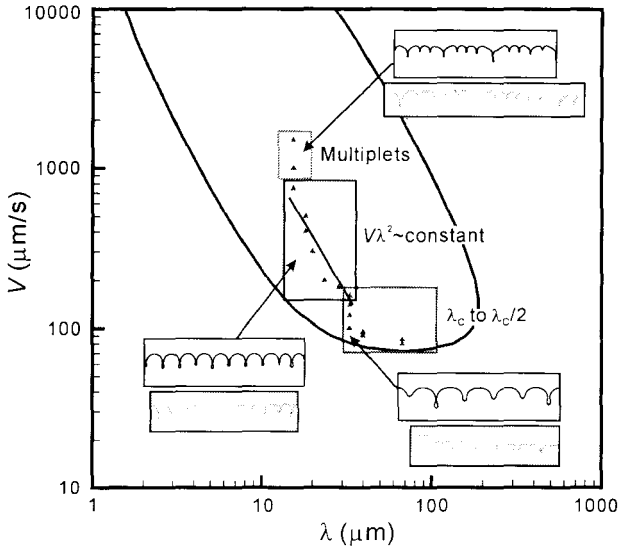

Fig. 10. Comparison of simulated wavelengths and speeds with the classic MS loop. Some observed shallow cells at $\lambda_c/2$, $V\lambda^2$~constant, and multiplets are illustrated.

quadruplet cells are highlighted for the sake of comparison. As shown, a large group of multiplets was also obtained experimentally. The complete transition from smaller-wavelength cells to multiplets is interesting, but had not previously been reported based on simulation or experimental results. The simulated morphological evolution caused by the change of speed from 750 μm/s to 1000 μm/s is illustrated in Fig. 8. As shown, the wavelength ($\sim\lambda_c/4$) remains about the same, and the multiplets emerge over with time. The wavelength remains the same up to V=1500 μm/s. In our experiment, the wavelength variation was similar to the simulated one shown in Fig. 7 (on average, λ=175 μm was obtained), and it became longer, which indicates that the long-cell region was approaching (Eshelman *et al.*, 1988). In other words, $V\lambda^2$~constant no longer held in this region. We also observed asymmetric cells similar to the ones reported by Rappel (1993). As shown in Fig. 9, this time-periodic local nonlinear behavior describes competitive growth between two cells; both simulation (left) and experimental (right) results are illustrated. Asymmetric cells may occur between two groups of multiplets, and the swing frequency is found to be a function of the pulling speed.

CONCLUSION

The whole morphological transition of shallow cells near the onset of instability for thin-film solidification of an SCN/acetone alloy has been illustrated for the first time based on the results of both quantitative phase field simulations and long-time scale experiments. The achieved phase field modeling shows good agreement with both the MS and WL theories for planar solidification. In addition, an anti-trapping current is introduced to improve the local partition at higher speeds. Long-time scale experiments at a constant speed near V_c indeed provide a means of observing the overall shallow cellular dynamics. To summarize the obtained results, the wavelength variations with the classic MS loop are plotted in Fig. 10. Both simulation and experimental results indicate four individual regions in the plot. With increasing pulling speed, transitions from planar to $\lambda_c \leftrightarrow \lambda_c/2$ bifurcation, $V\lambda^2$~constant, and then multiplet regions clearly result. In addition, during the transitions, global and local nonlinear dynamics, such as tip splitting, coarsening, pinching off, and swing asymmetric cells, are observed. Although the simulation and experimental results are in good qualitative agreement, simulating an alloy with a concentration comparable to those in the existing experiments is difficult because of the very long simulation time. Therefore, for one-to-one comparison to be possible, in addition to huge computing power, a quantitative phase field model that allows for the use of a thick interface is required.

ACKNOWLEDGEMENT

The authors are grateful for the financial support provided by the National Science Council of the Republic of China. Valuable comments from Profs. B. Billia, R. F. Sekerka, and R. Trivedi are gratefully acknowledged.

NOMENCLATURE

a	anti-trapping coefficient
c	atomic fraction
D	diffusivity, m^2/s
h	weighting function
H	domain height, μm
j_a	anti-trapping current flux, mol/m^2s
m	slope of liquidus line, K/(mol fraction)
M	mobility, $Km^3/(J\cdot s)$
k	segregation coefficient
S	volumetric entropy, $J/(Km^3)$
t	time, s
T	temperature, K
W	domain width, μm
x	coordinate, μm
y	coordinate, μm
V	pulling velocity, μm/s

Greek symbols

β	angle, rad

δ	interface thickness, μm
ε	interfacial energy, J/m^2
ϕ	phase field variable
γ	anisotropic intensity
η	anisotropic function
λ	wavelength, μm

Subscripts

0	far field
A	solvent
B	solute
c	critical value
eff	effective value
i	interface
L	liquid
S	solid

Superscript

*	dimensionless variables

REFERENCES

Ahmad, N. A., A. A. Wheeler, W. J. Boettinger, and G. B. McFadden, "Solute Trapping and Solute Drag in a Phase-Field Model of Rapid Solidification," *Phys. Rev. E*, **58**, 3436 (1998).

Aziz, M. J. and T. Kaplan, "Continuous Growth-Model for Interface Motion during Alloy Solidification," *Acta. Metall.*, **36**, 2335 (1988).

Bi, Z. Q. and R. F. Sekerka, "Phase Field Modeling of Shallow Cells during Directional Solidification of a Binary Alloy," *J. Cryst. Growth*, **237**, 138 (2002).

Boettinger, W. J. and J. A. Warren, "Simulation of the Cell to Plane Front Transition during Directional Solidification at High Velocity," *J. Cryst. Growth*, **200**, 583 (1999).

Eshelman, M. A. and R. Trivedi, "The Planar to Cellular Transition during the Directional Solidification of Alloys," *Acta Metall.*, **35**, 2443 (1987).

Eshelman, M. A., V. Seetharaman, and R. Trivedi, "Cellular Spacings .1. Steady-State Growth," *Acta Metall.*, **36**, 1165 (1988).

Jamgotchian, H., R. Trivedi, and B. Billia, "Array of Doublets – A Branch of Cellualr Solutions in Directional Solidification," *Phys. Rev. E*, **47**, 4313 (1993).

Karma, A., "Phase-Field Formulation for Quantitative Modeling of Alloy Solidification," *Phys. Rev. Lett.*, **87**, 115701 (2001).

Kopczynski, P., W. J. Rappel, and A. Karma, "Cellular Multiplets in Directional Solidification," *Phys. Rev. E*, **55**, R1282 (1997).

Kurowski, P., S. de Cheveigne, G. Faivre, and C. Guthmann, "Cusp Instability in Cellular Growth," *J. Phys.* (Paris), **50**, 3007 (1989).

Lan, C. W., C. C. Liu, and C. M. Hsu, "An Ddaptive Finite Volume Method for Incompressible Heat Flow Problems in Solidification," *J. Comp. Phys.* **178**, 464 (2002).

Lan, C. W., "Recent Progress of Crystal Growth Modeling and Growth Control," *Chem. Eng. Sci.*, **58**, 1437 (2004).

Lan, C. W. and C. J. Shih, "Efficient Phase Field Simulation of a Binary Dendritic Growth in a Forced Flow," *Phys. Rev. E*, **69**, 031601 (2004).

Lan, C. W., C. J. Shih, and W. T. Hsu, "Long-Time Scale Morphological Dynamics near the Onset of Instability during Directional Solidification of an Alloy," *J. Cryst. Growth*, **264**, 379 (2004).

Lee, J. T. C., K. Tsiveriotis, and R. A. Brown, "Spatiotemporal Chaos near the Onset of Cellular Growth during Thin-Film Solidification of a Binary Alloy," *J. Cryst. Growth*, **121**, 536 (1992).

Losert, W., B. Q. Shi, and H. Z. Cummins, "Evolution of Dendritic Patterns during Alloy Solidification: Onset of the Initial Instability," *Proc. Natl. Acad. Sci.* U.S.A., **95**, 431 (1998).

Mullins, W. W. and R. F. Sekerka, "Stability of a Planar Interface during Solidification of a Dilute Binary Alloy," *J. Appl. Phys.*, **35**, 444 (1964).

Provatas, N., N. Goldenfield, and J. Dantzig, "Adaptive Mesh Refinement Computation of Solidification Microstructures Using Dynamic Data Structures," *J. Comput. Phys.* **148**, 265 (1999).

Rappel, W. J., "Asymmetric Cell in Directional Solidification," *Phys. Rev. E*, **48**, 4118 (1993).

Trivedi, R. and K. Somboonsuk, "Pattern-Formation during the Directional Solidification of Binary-Systems," *Acta Metall.*, **33**, 1061 (1985).

Tsiveriotis, K. and R. A. Brown, "Nonlinear Local Dunamics of the Melt Crystal Interface of a Binary Alloy in Directional Solidification," *Phys. Rev. B*, **48**, 13495 (1993).

Ungar, L. H. and R. A. Brown, "Cellular Interface Morphologies in Directional Solidification - the One-Side," *Phys. Rev. B*, **29**, 1367 (1984).

Warren, J. A. and W. J. Boettinger, "Predition of Dendritic Growth and Microsegregation Patterns in a Binary Alloy Using the Phase-Field Method," *Acta Metall. Mater.*, **43**, 689 (1995).

Warren, J. A. and J. S. Langer, "Prediction of Dendritic Spacings in a Directional-Solidification Experiment," *Phys. Rev. E*, **47**, 2702 (1993).

(*Manuscript received Mar. 7, 2005, and accepted Jun. 9, 2005*)

薄膜合金固化過程淺細胞的型態轉變: 相場模擬與實驗觀察

施智仁　徐爲哲　藍崇文
國立台灣大學化學工程學系

摘　要

本文中我們首次以定量相場模擬琥珀腈/丙酮合金薄膜固化在接近 Mullins-Sekerka 不穩定區的型態轉變過程，並做長時間/長樣品的等拉速凝固實驗比較之。模擬結果從平整界面失穩到$\lambda_c \leftrightarrow \lambda_c/2$ 細胞分歧區與古典理論相當吻合；其中λ_c為臨界波長。在較高拉速區，我們並引入反向溶質通量來維持局部熱力學平衡，並發現 $V\lambda^2$ 約為常數的區域。最後在波長接近四分之一的臨界波長時，更有巒生細胞的出現。實驗中由於有限的熔區長度，在等拉速下有溶質累積，我們可觀察到類似模擬中變拉速（固定濃度）的型態轉變。模擬與實驗也同樣的觀察到細胞分裂、結合、溶質覆胞脫離與非對稱細胞等有趣的非線性行為。